1-1-2016

Defect graphene as a trifunctional catalyst for electrochemical reactions

Yi Jia
Griffith University

Longzhou Zhang
Griffith University

Aijun Du
Queensland University of Technology

Guoping Gao
Queensland University of Technology

Jun Chen
University of Wollongong, junc@uow.edu.au

See next page for additional authors

Defect graphene as a trifunctional catalyst for electrochemical reactions

Abstract

The defects derived by the removal of heteroatoms from graphene have been demonstrated, both experimentally and theoretically, to be effective for all three basic electrochemical reactions, e.g., oxygen reduction (ORR), oxygen evolution (OER), hydrogen evolution (HER). Density function theory calculations further reveal that the different types of defects are essential for the individual electrocatalytic activity for ORR, OER, and HER, respectively.

Publication Details

Jia, Y., Zhang, L., Du, A., Gao, G., Chen, J., Yan, X., Brown, C. L. & Yao, X. (2016). Defect graphene as a trifunctional catalyst for electrochemical reactions. Advanced Materials, 28 (43), 9532-9538.

Authors

Yi Jia, Longzhou Zhang, Aijun Du, Guoping Gao, Jun Chen, Xuecheng Yan, Christopher L. Brown, and Xiangdong Yao

Defect Graphene as a Tri-functional Catalyst for Electrochemical Reactions

By *Yi Jia*,[⊥] *Longzhou Zhang*,[⊥] *Aijun Du, Guoping Gao, Jun Chen, Xuecheng Yan, Christopher L. Brown* and *Xiangdong Yao* *

Dr. Y. Jia, L. Z. Zhang, X. C. Yan, Prof. X. D. Yao
Queensland Micro- and Nanotechnology Centre, Griffith University,
Nathan Campus, Queensland 4111, Australia
E-mail: x.yao@griffith.edu.au
G. P. Gao, Prof. A. J. Du
School of Chemistry, Physics and Mechanical Engineering, Queensland University of Technology, Brisbane, Queensland 4000, Australia
Prof. J. Chen
Intelligent Polymer Research Institute, ARC Centre of Excellence for Electromaterials Science, AIIM Facility, Innovation Campus, University of Wollongong, Wollongong, NSW 2522, Australia
Dr. Y. Jia, L. Z. Zhang, X. C. Yan, Prof. C. L. Brown, Prof. X. D. Yao
School of Natural Sciences, Griffith University, Queensland 4111, Australia
Prof. C. L. Brown
Environmental Futures Research Institute, Griffith University, Queensland 4111, Australia

[⊥] Y. Jia and L. Z. Zhang contributed equally.

Keywords: Defects, Graphene, Electrocatalyst, Oxygen reduction and evolution, Hydrogen evolution

The development of low cost, environmentally innocuous, efficient and durable electrocatalysts possessing the broad spectrum of functionality that is required for three key electrochemical reactions, hydrogen evolution (HER), oxygen reduction (ORR) and oxygen evolution (OER), is critically important for advancement in renewable energy conversion and storage.[1-6] Typical examples are the rechargeable air based battery, which combines ORR and OER, and the water splitting process combining HER and OER. The current spectrum of catalysts utilized for these fundamental electrochemical reactions are platinum (Pt) for ORR and HER and iridium (Ir) for applications in OER. Their 'rare earth' status and associated high cost renders them less than ideal materials for incorporation into bulk production scale devices that will be required for clean energy conversion and storage such as air cells and hydrogen production.[3, 5, 6] In addition,

the use of two different single function catalysts for ORR (Pt) and OER (Ir) respectively makes the air cell significantly more complex as it requires the combination of three electrodes.[5, 7]

Since the demonstration that metal free nitrogen doped (N-doped) carbon nanotubes can act as efficient catalysts in ORR, considerable interest has been directed to the assembly of carbon based metal free electrochemical catalysts.[8-11] Afterwards the early observations of catalytic activities of N-doped CNT systems, the chemistry has been expanded to incorporate other heteroatom doping/co-doping elements (such as B, S and P) into a range of carbon based systems, such as carbon nanotubes and more recently graphene.[12-14] Whilst thousands of papers have been published on the topic in recent years, the actual catalytic mechanism arising from the heteroatom doping still remains a topic of some debate.[15-19] For example, in N-doped carbon based assemblies, some reports have indicated that it is the pyridinic sp^2 nitrogen centre that provides the catalytically active sites for the ORR, whilst conversely, other reports have claimed that it is the graphitic (quaternary and sp^2) nitrogen centre that provides the catalytic activity. Currently there is no consensus on this point although a recent article in the prestigious journal Science strongly supports the mechanism of a pyridinic nitrogen based mechanism.[20] More importantly, enthusiasts of the N-doping catalytic model claim that it is the higher electronegativity of nitrogen over carbon that induces a partial positive charge in carbon atoms proximal to the nitrogen atoms and it is this charge polarization that is involved in the attraction and subsequent dissociation of adsorbed O_2 molecules. However, this rather simplistic mechanism does not explain other catalytically active heteroatom doped systems such as those that incorporate the group III element boron as the electro-negativity of boron is lower than that of nitrogen, and the group VI element sulfur, being comparable to that of carbon,[13] suggesting that there is some confusion to the actual catalytic mechanism of these doped systems.

Recently, we investigated the relationship between catalytic activity of N-doped systems and the nitrogen content in the ORR by carbonization of a N-rich PAF-40.[21] In this study we observed an inverse relationship between N-content of the system and catalytic activity, i.e. the

lower the nitrogen content the higher the ORR activity in a nitrogen range of 0.21~2.11 atom %N (negative correlation of the relationship). This is in direct contrast to the N-doped theory vide supra in which there should be positive correlation of catalytic activity *vs*. nitrogen content if the N-doping theory is valid. Furthermore, we subsequently carbonized a Zn-MOF removing all of the Zn[22] to yield a derived carbon containing only C and O, without any active doping elements (e.g. N, B, P or S) as determined by XPS. The derived pure carbon exhibited excellent ORR activity, in contrast to the requirements of the heteroatom doping mechanism (that is no doping, no activity). Accordingly, we recently presented a mechanism for ORR that is dependent on carbon defects within the structure and supported or hypothesis with theoretical calculations.[21] However, we had not directly observed the topological defects on the MOF derived carbon samples due to the resulting complex 3-D structure obtained after removal of the zinc and carbonization.[21, 22]

Here, we report the assembly of a 2D graphene material possessing carbon defects (DG) obtained via a facile nitrogen removal procedure from a N-doped precursor. We subsequently investigated the ORR activity of this material coupled with direct observations of the defects using high-resolution transmission electron microscopy (HRTEM). As the process may create different types of defects, we hypothesized that the defective graphene may be also functional for other catalytic reactions such as OER and HER. Our theoretical calculations support this hypothesis and the experimental work confirms the triple functions of the DG material. The simple approach we utilized to synthesize a triple functional material possesses overwhelming advantages over the current complicated fabrication process of bi-functional catalysts (multi-step co-doping and hybridization).[10, 14]

A cartoon illustrating the removal of the doping element is outlined in **Figure 1**a. It is anticipated that various defects (pentagons, heptagons and octagons) are formed from carbon atom reconstruction arising from multiple single-atom vacancies induced after N-atoms are removed through heat treatment.[21] X-ray photoelectron spectroscopy (XPS) was used to

confirm the loss of nitrogen dopant after heat treatment. It is notable that the N1s peak was detected with ~4 at% nitrogen in the starting N-doped graphene (NG) (Figure 1b). High resolution analysis of the N1s spectra after peak deconvolution further reveals that three main peaks can be fitted at 398.3, 399.6 and 401.0 eV, which can be ascribed to pyridinic, pyrrolic and graphitic nitrogens, respectively (Figure 1c).[16] XPS analysis of the material after heat treatment confirms the absence of the nitrogen atoms in the DG material (Figure 1b and c). As the XPS only can characterize the composition on the surface, element analysis was further used to reveal the N content in whole of NG and DG, respectively. The results show that the contents of N are ~ 4.3 wt% (3.7 at%) and ~ 0.8 wt% (0.7 at%) for NG and DG, respectively, indicating that the carbon inside contains a very small amount of N. However, we do not think the activity is from these N because there was no N on the surface of carbon and the reactions rightly occurred on the surface. Furthermore, two of our previous works have supported the defect but not N is functional: 1) N-doped activated carbon (AC) has been demonstrated to be non-active for electrochemical reactions, but the defective AC is highly active for ORR and HER;[23] 2) we use Zn removal method to create defects on carbon, which shows highly active for ORR. The whole process did not touch any sources of N and it was confirmed that there is no N in the carbon.[22] The process to form the defect material can be attributed to subtraction of nitrogen atoms under high energy conditions resulting in the formation of vacant sites. These sites subsequently structurally rearrange to minimize energy via reconstruction of the carbon lattice forms rings of various sizes such as pentagons, heptagons, even octagons.[24, 25] Raman analysis clearly shows the variation in the intensity of the D and G bands between the NG and DG samples (Figure 1d). For graphene, the intensity of D band is lower than that of G band with I_D/I_G ratio of 0.89 (Figure 1d inset), suggesting the high regularity of carbon structure possessing relatively fewer defects. Incorporation of nitrogen heteroatoms doped into the graphene sheets, results in an increase in D band intensity, indicating the disruption of hexagonal structure[8-11] and the introduction of some defect sites. Removal of the nitrogen

doping atoms results in a further increase in defects as shown by the increase in the ratio of I_D/I_G continually from 1.06 to 1.13 (Figure 1d inset), suggesting the more widespread formation defective domains.[24, 25]

To verify the Raman data, aberration-corrected high-resolution transmission electron microscopy (AC-HRTEM) was used to actually visualize the defects regions of the material. At low magnification (Figure 1e and Supplementary Figure S1a, b), the representative images of the DG material revealed the formation of holes in the graphene sheet presumably resulting from the removal of nitrogen. Not surprisingly, various structural defects (pentagons, heptagons and octagons) with different combinations such as 585, 75585 (Figure 1f) and 5775 (Supplementary Figure S1c, d) were observed proximal to the lattice vacancies. It is perhaps not surprising that the structural defects mainly dominate on the edge of holes, while the normal hexagon graphene structure predominates in the bulk regions of the material. The evolution of the G-NG-DG structural transition was investigated using atomic force microscopy (AFM) and this technique highlighted that removal of doped N atoms leads to some localized destruction of graphene structure (Figure 1g and Supplementary Figure S2c-e). The thickness of the defect material as measured by edge analysis in the AFM was observed to be similar as original graphene starting material at ~ 0.6 nm, which is consistent with the TEM results. We propose that it is these defects that are fundamental in enhancing the electrocatalytic activity of the material, presumably due to the local modulated electronic environment associated with the defects.[24-26] Also important is that as these defects perturb the surface properties of the graphene, they induce other catalytic effects such as changes in specific surface area and surface hydrophobicity (contact angle of 44.3° (Supplementary Figure S4)) improving catalytically beneficial wetting properties.[3-5] When combined these surface changes (Supplementary Figure S3) it would be beneficial for mass transportation in an aqueous electrolyte.[5,6,10,12,18]

The evaluation of the electrocatalytic activity of the DG was initially carried out using the oxygen reduction reaction (ORR) in O_2-saturated 0.1 M KOH aqueous solution at room temperature. The linear scan voltammogram (LSV) curves in **Figure 2**a confirm the efficient ORR of DG, with a positive onset potential of 0.91 V versus reversible hydrogen electrode (RHE) and a half-wave potential of 0.76 V versus RHE. These values are comparable to most previous reported metal free ORR catalysts (Refs in Supplementary Table S1). In terms of half-wave potential, limiting current density and Tafel slope, it is demonstrated that the DG shows much higher activity than that of NG (Figure 2a and Supplementary Figure S5a), indicating the defects are essential for the ORR in this system. The electron transfer number per oxygen molecule (n) for DG in ORR was determined to be 3.87 by Koutecky-Levich (K-L) plots (Supplementary Figure S5b), indicating a 4-electron pathway reaction.[3] The durability of the DG over the course of the experiments is also excellent and better than Pt/C (Supplementary Figure S5c). More interestingly, the DG catalyst also exhibited superior ORR activity in acidic electrolyte (0.1 M H_2SO_4). As seen in Supplementary Figure S6, the DG catalyst displays high activity at high voltages, which is superior to that of the N doped graphene (NG) and pristine graphene (G) catalysts in acidic electrolyte. In addition, it is noticed that although the electrochemically active surface area (EASA) of DG is lower than that of G, DG shows much higher current density, implying that EASA is not the only contributor to the enhanced kinetics (Supplementary Figure S7).

Given the encouraging data obtained in the ORR experiments, we continued on to examine the activity of this materials for the OER and HER experiments. In the OER experiment, the DG material exhibited an activity remarkably higher than that of pristine graphene (no activity) and NG, with a potential of 1.57 V under the current density of 10 mA cm^{-2} and a lower Tafel slope (97 mV dec^{-1}). This activity is comparable to Ir/C (a commercial OER catalyst) (Figure 2b and Supplementary Figure S8a). The OER catalytic activity of DG is also comparable to the

reported doped or hybrid non-precious metal electrodes in terms of onset potential and current density (Refs in Supplementary Table S2). Furthermore, the DG also shows a good OER durability (Supplementary Figure S8b).

Also, the DG shows significantly improved HER activities over both G and NG, in both acid and alkaline solutions (Figure 2c and d). In a 0.5M H_2SO_4 solution, the operating potentials at a current density of -10 mA cm^{-2} are measured to be -0.42 V for G, -0.35 V for NG, and -0.15 V for DG, respectively. The DG also shows excellent kinetic properties with the lowest Tafel slope at 55 mV dec^{-1} and high stable chronopotentiometric performance at current densities of 5 and 10 mA cm^{-1} (Supplementary Figure S8c, d). These values outperform most previous reported metal free HER catalysts (Refs in Supplementary Table S3), and close to some benchmarking metal based catalysts for HER such as Mo_xS_y and Ni_xP_y.[27-29] Impressively, DG shows excellent activity in 1 M KOH solution, in fact, it is much better than that of state-of-the-art non-metal HER electrocatalysts currently reported (Refs in Supplementary Table S3). This observation is particularly exciting as the HER in alkaline solution is very important for the overall water splitting process[30] and this observation is in contrast to the N-doped material (NG) which has limited HER performance in alkaline media (Figure 2d and Supplementary Figure S8e, f).

In summary, the defect graphene (DG) material outlined here is not only functional for ORR but also for the OER and HER, and the activity of the material is significantly higher than that of the parent NG for all the three basic electrochemical reactions.

In an attempt to understand the underlying catalytic mechanisms displayed by this defect graphene, we undertook as series of density function theory (DFT) experiments to better describe the catalytically active sites for the ORR, OER and HER processes (more computational details in the Supplementary information). Four computational models were derived from the experimentally observed types of defect observed in the NG material, i.e. edge

pentagon, 585, 7557, and 5775 defects. Analysis of the frontier molecular orbitals revealed that that the HOMO and LUMO orbitals are predominantly distributed on the edge atoms of the graphene holes (Supplementary Figure S9). Once the edge pentagon, 585 defect, 7557 defect are introduced, edge atoms around the defect contributed to the HOMO/LUMO orbitals except for the 5775 defect (Supplementary Figure S9). As the catalytic reaction is highly correlated with HOMO/LUMO orbital distributions, the 5775 defect is not active for the ORR, OER and HER reactions. Only edge pentagon, 585 defect, and 7557 defect are plotted with defect atoms labeled and highlighted in green color (**Figure 3**a-c). The minimum energy pathways were calculated for the ORR, OER and HER, and only five defect atomic sites (5-1, 585-1, 585-3, 7557-1 and 7557-4) with the highest catalytic activity were selected (Figure 3d-f). The most active sites for the ORR under pH=13 is edge 5-1 with a smallest activation barrier of 0.470 eV, followed by 7557-1 with a barrier of 0.483 eV (Figure 3d and Supplementary Table S4). Meanwhile, the minimum potential for the OER at pH=14 is 0.945 V and 0.948 V for 5-1 and 585-1 defect, respectively (Figure 3e and Supplementary Table S4). The most active sites for the HER is 7557-4 ($\Delta G^0_{H*} = -0.187\ eV$) (Figure 3f and Supplementary Table S4). Remarkably, the edge carbons in all three systems (5-1, 585-1, and 7557-1) demonstrate the superior activities for both ORR and OER. Previously, edge effects have been considered to improve the catalytic activities of the graphene.[26] The defects at the edge (pentagon, 585, and 7557) reported in this work could further significantly enhance the catalytic activities (Supplementary Figure S10). It should be noted that the hydrogen binding energy on most edge carbons are too strong for the HER, while the conjunction carbons (585-3 and 7557-4) possess a desired hydrogen binding energy and thus demonstrate excellent HER performance.

Inspired by the notable half-cell performance of the DG material in the ORR and OER, 0.1 mg of the DG material was pasted on to a porous carbon fiber paper (CFP) and this was subsequently used as a cathode catalyst to evaluate the full-cell potential of the material in a

split test cell (EQ-STC-MTI) for a rechargeable zinc-air battery (**Figure 4**a and inset). The interior components and construction of the cell is shown in Figure 4b. The electrolyte used in the experiment was 6 M KOH and 0.2 M zinc acetate (dissolved in KOH to form zincate, $Zn(OH)_4^{2-}$) to ensure reversible Zn electrochemical reactions at the anode.[5] To determine the longer term stability of the system, charging and discharging cycles (300 s in each cycle) at different current rates using the recurrent galvanic pulse method[5] were employed (Figure 4c). The DG material exhibited respectable durability at current densities of both 5 mA mg^{-1} and 10 mA mg^{-1}. After 90 charge/discharge cycles, the charge potentials still held at 1.90 V and 1.92 V respectively, while the discharge potentials declined only slightly. Furthermore, the potentials of charge/discharge and power densities with increasing current densities were measured. Remarkably, this DG catalyst electrode delivers a current density of ~100 mA mg^{-1} at the discharging voltage of 1 V and a peak power density of ~154 mW mg^{-1} at a current density of 195 mA mg^{-1}, which are comparable to those of the reported Pt/C counterparts (Figure 4d).[4, 5, 31] To meet specific energy and/or power needs for various practical applications, multiple Zn–air batteries can be integrated into series or parallel circuits (Supplementary Movie). As exemplified in Figure 4e, two Zn-air batteries can be connected in series to generate a sufficiently high open circuit potential (OCP) of 2.63 V to power a LED light (~ 2 V). In the other case of enhancing current output, two Zn-air batteries can also be connected in parallel to generate a sufficiently high circuit current of 32.5 mA to drive an electrical model vehicle (Figure 4f).

To summarize, the defects derived by the removal of heteroatoms from graphene have been demonstrated, both experimentally and theoretically, to be effective for all three basic electrochemical reactions, e.g. ORR, OER and HER. The activities of the DG for all three reactions are much better than the N-doping graphene. To our best knowledge, tri-functional metal free catalyst based on defect mechanism is firstly reported and confirmed. In view of the

excellent activity, we demonstrated the DG catalyst for Zn-air battery. The Zn-air battery suggests that the DG has very stable charge and discharge voltages, high current and power density, which is comparable to Pt. The defective carbons with triple functions will have many potential applications and we believe the defect mechanism will be useful for designing next generation of catalysts for electrocatalysis.

Experimental

The synthesis of N-graphene: N-graphene was prepared from pristine graphene using thermal annealing method. Typically, the graphene was mixed with melamine (mass ration is 1:1), and annealed at 700 °C for 2 hours with a ramp rate of 5 °C under nitrogen atmosphere. Before heating, the system was purged for two hours with nitrogen gas to ensure the removal of oxygen from the furnace. The as prepared sample was denoted as NG.

The synthesis of D-graphene: D-graphene was obtained from the N-graphene precursor. In a typical experiment, N-graphene was annealed at 1150 °C for 2 hours with a ramp rate of 5 °C under an atmosphere of nitrogen that promote nitrogen atom subtraction from the sample and produce the topological defects. To simplify the synthesis, the above two processes can be combined in one step. The as prepared sample was denoted as DG.

Characterization: X-ray diffraction (XRD) patterns were acquired at room temperature using D/MAX 2550 VB/PC. Raman spectrum was recorded on a Rennishaw InVia spectrometer with a model 100 Ramascope optical fibre instrument. X-ray photoelectron spectrum (XPS) data was collected from a Kratos Axis ULTRA X-ray photoelectron spectrometer, and the binding energy of the C 1s peak at 284.8 eV was used as an internal reference. Flash EA 1112 CHNS-O analyzer (Thermo Electron Corp., USA) was applied to quantify the nitrogen content in samples. Transmission electron microscopy (TEM) images were collected from TECNAI 12 and probe-

corrected JEOL ARM200F with acceleration voltages of 120 kV and 80 kV, respectively. HAADF images were acquired with inner and outer collection angles of 50 to 180 mrad respectively, while BF images were acquired with a maximum collection angle of 11 mrad. All images were acquired with a 60 ms dwell time and convergence angle of 25 mrad, resulting in a probe size of 1 A and a current of 30 pA. Bruker Multimode 8 Atomic force microscope (AFM) was applied to examine the topography of the nanosheets deposited on freshly cleaved micas.

Electrochemical test: All the electrochemical tests were performed in a conventional three-electrode system at an electrochemical station (CHI 760E), using Ag/AgCl (saturated KCl solution) electrode as the reference electrode, Pt mesh as the counter electrode and glassy carbon (GC) electrode as the working electrode. All potentials were referred to the reversible hydrogen electrode (RHE) by following calculations: E (vs RHE) = E (vs Ag/AgCl) + 0.197+0.059pH.

ORR measurement: 1 mg of the catalyst was dispersed into the 1 mL mixed solution of distilled water (680 μL), ethanol (300 μL) and Nafion Solution (5%, 20 μL). Then, 10 μL of the mixture was dropped onto a polished glassy carbon electrode (4 mm in diameter) after sonication for at least 60 min to form a homogeneous ink. The loaded electrode was placed in a 60 °C oven for 10 min to dry and allow to cool to room temperature before performing tests. Both prior to the test (for at least 30 min) and during the experiment, the electrolyte (0.1 mol/L KOH solution) was saturated with O_2 via a bubbler. The data was recorded at the scan rate of 100 mV/s once the system achieved equilibrium. The rotating speed of the working electrode was increased from 400 rpm to 2500 rpm at the scan rate of 10 mV/s in O_2-saturated 0.1 M KOH solution during the linear sweep voltammetry test.

HER and OER measurements: Typically, 4 mg of sample was dispersed in 1 mL mixed solution of distilled water (680 μL), ethanol (300 μL) and Nafion®117 Solution (5%, 20 μL), followed

by at least 60 min sonication to form a homogeneous ink. Then 5 μl of the solution was loaded onto the GC electrode of 3 mm in diameter. The final loading for all catalysts and commercial Pt/C electrocatalysts on the GC electrodes was about 0.283 mg/cm^2. Linear sweep voltammetry with scan rate of 5 mV/s was conducted in 1M KOH or 0.2M H_2SO_4. Chronopotentiometry measurement (j = 5 mA/cm^2 and 10 mA/cm^2) was performed to evaluate the long-term stability of the system.

Zinc-air battery test: DG catalyst was loaded on foam carbon fiber paper (the cathode) to achieve the mass density of 0.1 mg/cm^2, functioned as cathode. Whatman glass microfibre filter was used as separator and Goodfellow Zinc foil was utilized as the anode. All the tests were proceeded on split test cell (MTI). Oxygen was bubbled through the system for at least 10 minutes to saturate the reaction chamber and this was maintained throughout the experiment.

Acknowledgements
We thank the financial support from Australia Research Council (ARC). Y. J. also thanks the Griffith University Postdoctoral and Research Fellowship and Griffith University New Research Grant. The authors acknowledge Hua Chen for her help with the atomic force microscope (AFM) analysis. ((Supporting Information is available online from Wiley InterScience or from the author)).

Received: ((will be filled in by the editorial staff))
Revised: ((will be filled in by the editorial staff))
Published online: ((will be filled in by the editorial staff))

[1] R. Bashyam, P. Zelenay, *Nature* **2006**, *443*, 63.

[2] G. Wu, K. L. More, C. M. Johnston, P. Zelenay, *Science* **2011**, *332*, 443.

[3] L. M. Dai, Y. H. Xue, L. T. Qu, H. J. Choi, J. B. Baek, *Chem. Rev.* **2015**, *115*, 4823.

[4] J. T. Zhang, Z. H. Zhao, Z. H. Xia, L. M. Dai, *Nat. Nanotechnol.* **2015**, *10*, 444.

[5] Y. G. Li, H. J. Dai, *Chem. Soc. Rev.* **2014**, *43*, 5257.

[6] Y. Jiao, Y. Zheng, M. T. Jaroniec, S. Z. Qiao, *Chem. Soc. Rev.* **2015**, *44*, 2060.

[7] Y. G. Li, M. Gong, Y. Y. Liang, J. Feng, J. E. Kim, H. L. Wang, G. S. Hong, B. Zhang, H. J. Dai, *Nat. Commun.* **2013**, *4*, 7.

[8] K. P. Gong, F. Du, Z. H. Xia, M. Durstock, L. M. Dai, *Science* **2009**, *323*, 760.

[9] Y. F. Tang, B. L. Allen, D. R. Kauffman, A. Star, *J. Am. Chem. Soc.* **2009**, *131*, 13200.

[10] Y. Zheng, Y. Jiao, J. Chen, J. Liu, J. Liang, A. Du, W. M. Zhang, Z. H. Zhu, S. C. Smith, M. Jaroniec, G. Q. Lu, S. Z. Qiao, *J. Am. Chem. Soc.* **2011**, *133*, 20116.

[11] Y. Zhao, R. Nakamura, K. Kamiya, S. Nakanishi, K. Hashimoto, *Nat. Commun.* **2013**, *4*, 7.

[12] Y. B. Li, H. M. Zhang, Y. Wang, P. R. Liu, H. G. Yang, X. D. Yao, D. Wang, Z. Y. Tang, H. J. Zhao, *Energy Environ. Sci.* **2014**, *7*, 3720.

[13] Y. Zheng, Y. Jiao, L. H. Li, T. Xing, Y. Chen, M. Jaroniec, S. Z. Qiao, *ACS Nano* **2014**, *8*, 5290.

[14] Y. Ito, W. T. Cong, T. Fujita, Z. Tang, M. W. Chen, *Angew. Chem.-Int. Edit.* **2015**, *54*, 2131.

[15] L. T. Qu, Y. Liu, J. B. Baek, L. M. Dai, *ACS Nano* **2010**, *4*, 1321.

[16] L. F. Lai, J. R. Potts, D. Zhan, L. Wang, C. K. Poh, C. H. Tang, H. Gong, Z. X. Shen, L. Y. Jianyi, R. S. Ruoff, *Energy Environ. Sci.* **2012**, *5*, 7936.

[17] W. Ding, Z. D. Wei, S. G. Chen, X. Q. Qi, T. Yang, J. S. Hu, D. Wang, L. J. Wan, S. F. Alvi, L. Li, *Angew. Chem.-Int. Edit.* **2013**, *52*, 11755.

[18] H.-W. Liang, X. Zhuang, S. Bruller, X. Feng, K. Mullen, *Nat. Commun.* **2014**, *5*, 4973.

[19] T. Xing, Y. Zheng, L. H. Li, B. C. C. Cowie, D. Gunzelmann, S. Z. Qiao, S. M. Huang, Y. Chen, *ACS Nano* **2014**, *8*, 6856.

[20] D. H. Guo, R. Shibuya, C. Akiba, S. Saji, T. Kondo, J. Nakamura, *Science* **2016**, *351*, 361.

[21] H. Y. Zhao, C. H. Sun, Z. Jin, D. W. Wang, X. C. Yan, Z. G. Chen, G. S. Zhu, X. D. Yao, *J. Mater. Chem. A* **2015**, *3*, 11736.

[22] X. J. Zhao, X. Q. Zou, X. C. Yan, C. L. Brown, Z. G. Cheng, G. S. Zhu, X. D. Yao, *Inorganic Chemistry Frontiers* **2016**, *3*, 417.

[23] X. C. Yan, Y. Jia, T. Odedairo, X. J. Zhao, Z. Jin, Z. H, Zhu and X. D. Yao, *Chem. Commun.* **2016**, *52*, 8156.

[24] F. Banhart, J. Kotakoski, A. V. Krasheninnikov, *ACS Nano* **2011**, *5*, 26.

[25] J. Kotakoski, A. V. Krasheninnikov, U. Kaiser, J. C. Meyer, *Phys. Rev. Lett.* **2011**, *106*, 4.

[26] L. P. Zhang, Q. Xu, J. B. Niu, Z. H. Xia, *Phys. Chem. Chem. Phys.* **2015**, *17*, 16733.

[27] J. Kibsgaard, T. F. Jaramillo, F. Besenbacher, *Nat. Chem.* **2014**, *6*, 248.

[28] E. J. Popczun, J. R. McKone, C. G. Read, A. J. Biacchi, A. M. Wiltrout, N. S. Lewis, R. E. Schaak, *J. Am. Chem. Soc.* **2013**, *135*, 9267.

[29] Y. G. Li, H. L. Wang, L. M. Xie, Y. Y. Liang, G. S. Hong, H. J. Dai, *J. Am. Chem. Soc.* **2011**, *133*, 7296.

[30] X. X. Zou, X. X. Huang, A. Goswami, R. Silva, B. R. Sathe, E. Mikmekova, T. Asefa, *Angew. Chem.-Int. Edit.* **2014**, *53*, 4372.

[31] Z. Chen, A. P. Yu, D. Higgins, H. Li, H. J. Wang, Z. W. Chen, *Nano Lett.* **2012**, *12*, 1946.

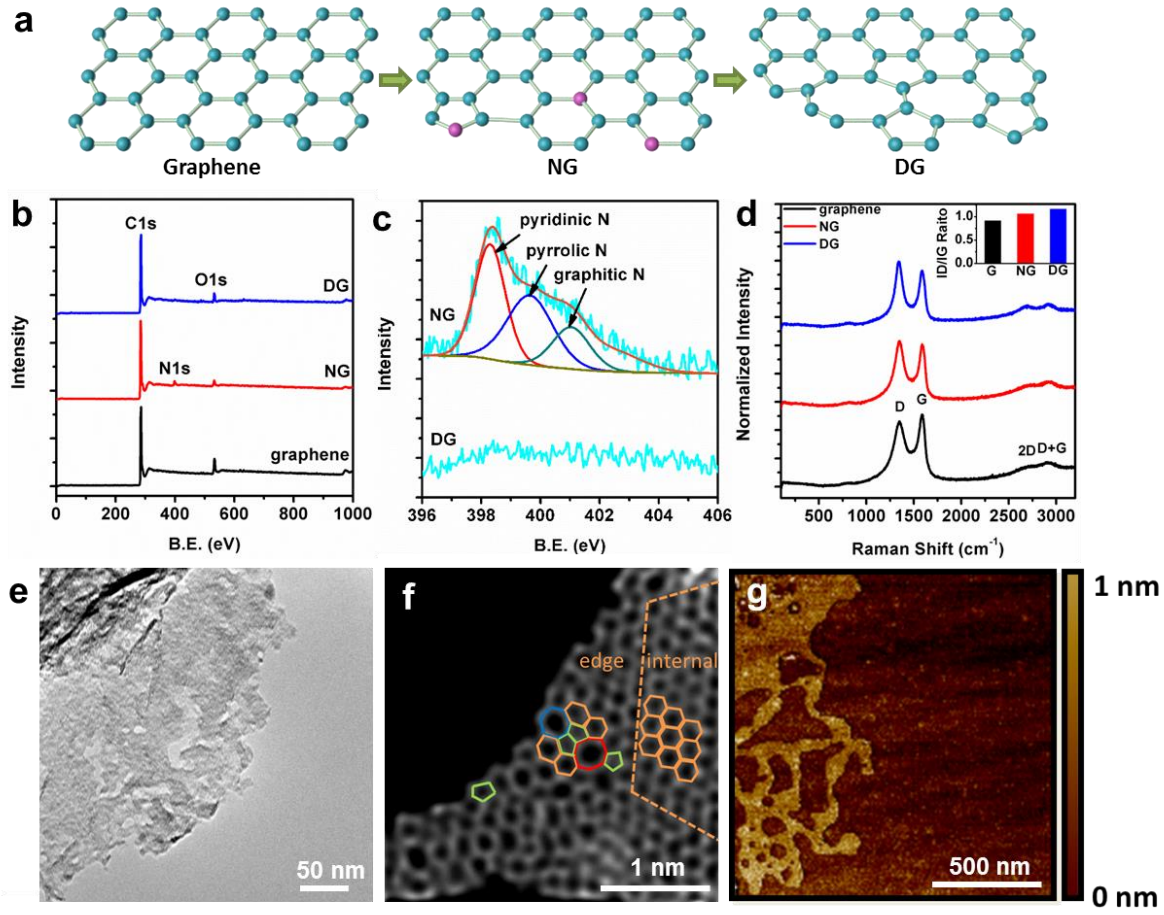

Figure 1. Characterizations of the resulting samples. (a) The schematic of the formation of DG. (b) XPS patterns of the pristine graphene, NG and DG. (c) High resolution of N1s spectra of NG and DG. (d) Raman patterns of pristine graphene, NG and DG. (e) The transmission electron microscopy (TEM) image of DG with an acceleration voltage of 120 kV. (f) HAADF image of DG with an acceleration voltage of 80 kV. Hexagons, pentagons, heptagons and octagons were labelled in orange, green, blue and red respectively. (g) The atomic force microscopy image of DG.

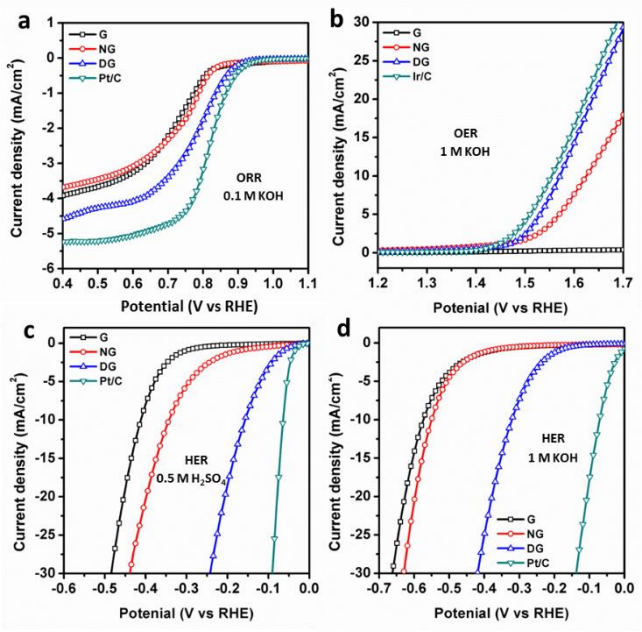

Figure 2. Linear sweeping voltammetry curves of the pristine graphene, NG and DG. (a) Oxygen reduction reaction. (b) Oxygen evolution reaction. (c) Hydrogen evolution reaction in acid and (d) alkaline solution, respectively.

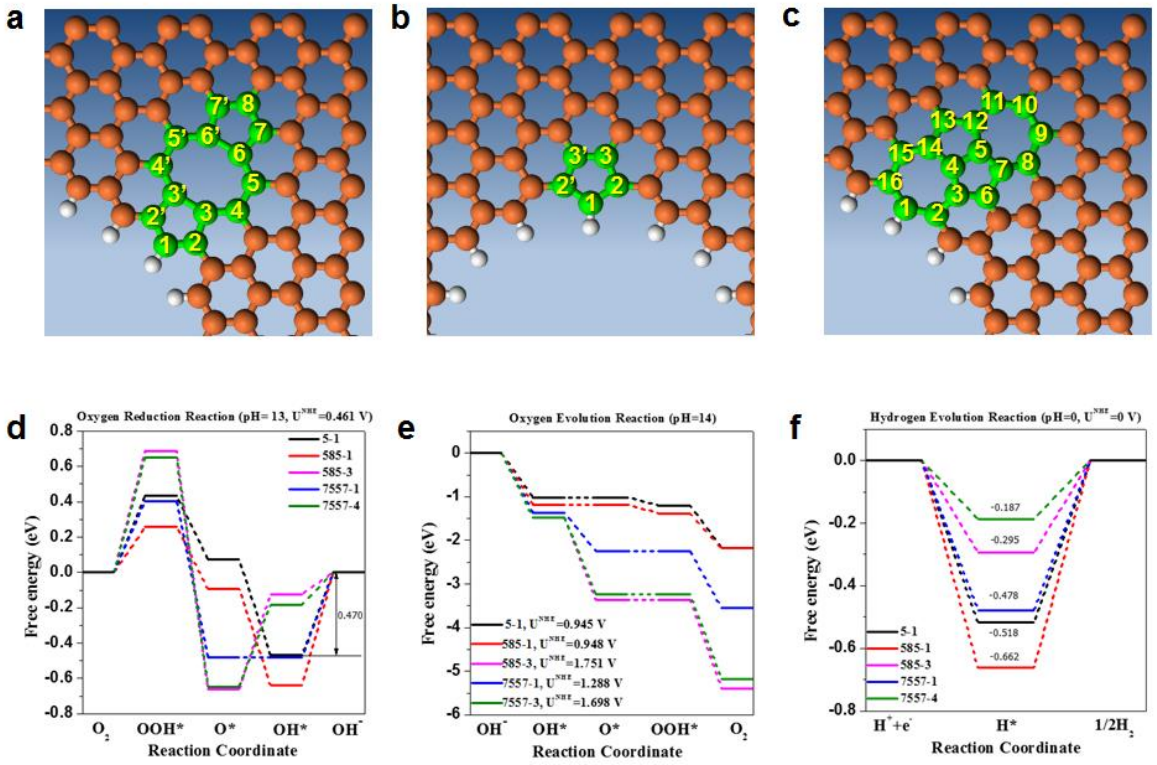

Figure 3. Mechanism study of tri-functionality in defective graphene for ORR, OER and HER. (a) Edge pentagon. (b) 5-8-5 defect. (c) 7-55-7 defect. (d-f) Schematic energy profiles for the ORR pathway, the OER pathway and the HER pathway on defective graphene in alkaline/acidic media. To improve legibility, 'OH-' was omitted from the labels.

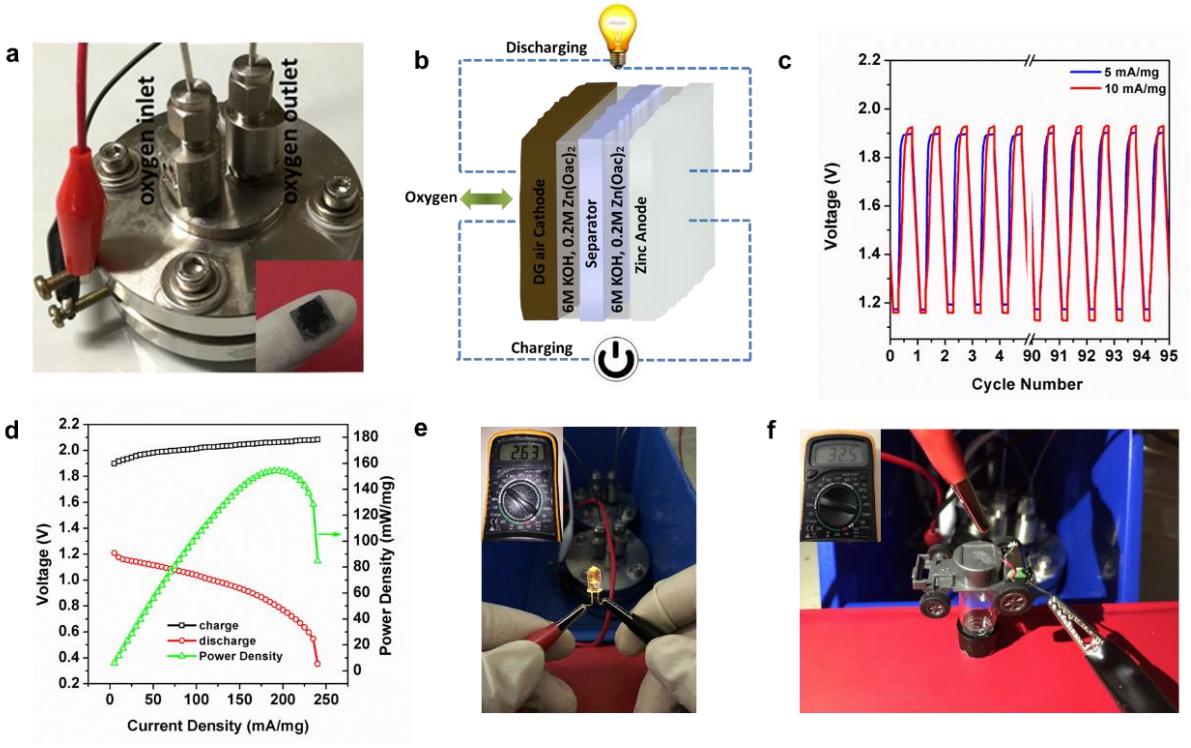

Figure 4. Potential applications of the DG. (a) Two electrodes Zn-air batteries testing device. (b) A schematic of interior assembling construction of the cell. (c) Performance of the battery charge–discharge cycling at 5 and 10 mA/mg, respectively. (d) Charge and discharge polarization curves and its output power density curve. (e) LED light (~ 2 V) powered by two zinc-air batteries in series. The inset is the voltage, unit: V. (f) Electrical vehicle model powered by two zinc-air batteries in parallel. The inset is the current, unit: mA.

The table of contents entry

The defects derived by the removal of heteroatoms from graphene have been demonstrated, both experimentally and theoretically, to be effective for all three basic electrochemical reactions, e.g. ORR, OER and HER. DFT calculations further reveal that the different types of defects are essential for the individual electrocatalytic activity for ORR, OER, and HER, respectively.

Keyword: Defects, Graphene, Electrocatalyst, Oxygen reduction and evolution, Hydrogen evolution

Yi Jia,[⊥] Longzhou Zhang,[⊥] Aijun Du, Guoping Gao, Jun Chen, Xuecheng Yan, Christopher L. Brown and Xiangdong Yao*

Defect Graphene as a Tri-functional Catalyst for Electrochemical Reactions

TOC Figure